

Device Activity Detection and Channel Estimation for Millimeter-Wave Massive MIMO

Yinchuan Li, *Member, IEEE*, Yuancheng Zhan, Le Zheng, *Senior Member, IEEE*, Xiaodong Wang, *Fellow, IEEE*

Abstract—Millimeter-Wave Massive MIMO is important for beyond 5G or 6G wireless communication networks. The goal of this paper is to establish successful communication between the cellular base stations and devices, focusing on the problem of joint user activity detection and channel estimation. Different from traditional compressed sensing (CS) methods that only use the sparsity of user activities, we develop several Approximate Message Passing (AMP) based CS algorithms by exploiting the sparsity of user activities and mmWave channels. First, a group soft-thresholding AMP is presented to utilize only the user activity sparsity. Second, a hard-thresholding AMP is proposed based on the on-grid CS approach. Third, a super-resolution AMP algorithm is proposed based on atomic norm, in which a greedy method is proposed as a super-resolution denoiser. And we smooth the denoiser based on Monte Carlo sampling to have Lipschitz continuity and present state evolution results. Extensive simulation results show that the proposed method outperforms the previous state-of-the-art methods.

Index Terms—Compressed sensing, atomic norm, approximate message passing, millimeter-Wave, massive connectivity, state evolution, machine-type communications, massive multiple-input multiple-output (MIMO).

I. INTRODUCTION

A. Motivation

Massive connectivity is common in beyond 5G (B5G) or 6G wireless communication networks, with profound implications for Internet of Things (IoT) and Machine Type Communications (MTC). In this case, each cellular base station (BS) is connected to a large number of devices (on the order of 10^4 to 10^6). However, only a few of these large numbers of devices are usually active. Since to save power, the device is in a sleep state most of the time, and will not be activated when it is not triggered [1]–[3]. For such networks, accurate user activity detection and channel estimation are crucial to establish successful communication between BS and devices.

B. Prior Works

At beginning, the traditional cellular networks is based on arranging active devices into time or frequency domains. The

drawback is that the overhead is huge, because a large number of occasionally active users need to be scheduled on a separate control channel. To address this problem, a method based on random access protocol [4], [5] is proposed, the main idea of this kinds of contention-based methods is that the orthogonal signature sequence sent to the BS is randomly selects by each active user, if the selected preamble is not used by another user, then the connection is established. However, for a large number of devices, collisions are unavoidable, so contention resolution is required. Therefore, unlicensed non-orthogonal user access schemes are very popular. The main function of the non-orthogonal pilot sequence is to improve the detection performance under the condition of a large number of devices and a limited coherence time of the channel. Afterwards, the base station completes user activity detection and channel estimation based on the pilot sequences sent by active users to the BS simultaneously.

Furthermore, the sparsity in user activity pattern in these systems can be exploited to formulate compressed sensing (CS) problems [6]–[13]. In [6], [7], under the condition that the channel state information (CSI) is well performed at the BS, a user activity and data detection algorithm is proposed based on sparse structures.

For the case that CSI is not available at the BS, a modified Bayesian compressed sensing method is proposed in [8] for jointly user activity detection and channel estimation. Aiming at similar problems, [9] based on compressed sensing techniques [10]–[12], adopts methods such as basis pursuit to denoise and jointly decode information in orthogonal frequency division multiplexing (OFDM) systems. An algorithm [14] based on Bayesian learning is developed, utilizing proposed hyper-priors to capture structural signal characteristics and appropriate approximations to facilitate algorithm derivation.

Unfortunately, none of the above works has conducted strict performance analysis for large-scale connectivity non-orthogonal multiple access schemes. With the development of the approximate message passing (AMP) algorithm [15], the state evolution (SE) has shown its benefit for performance analysis in compressed sensing problem. Therefore, the AMP algorithm is recently used for activity detection and channel estimation problems [13], [16]. The advantage of the AMP algorithm is that it can perform state evolution analysis, and relevant conclusions can be used to model missed detection and false positive probability. However, the analysis in [13], [16] is quite involved. To improve this, [1], [2] simplifies the related characterization under the assumption of a large number of BS antennas. Furthermore, an important conclusion is drawn that the channel estimation error is much more restric-

Y. Li is with the Electrical Engineering Department, Columbia University, New York, NY 10027, USA (e-mail: yinchuan.li.cn@gmail.com).

Y. Zhan is with the School of Electrical and Electronic Engineering, Nanyang Technological University, Singapore 639798 (e-mail: zhan0530@e.ntu.edu.sg).

Le Zheng is with the Radar Research Laboratory, School of Information and Electronics, Beijing Institute of Technology, Beijing 100081, China. He is also with the Chongqing Innovation Center, Beijing Institute of Technology, Chongqing 401120, China (e-mail: le.zheng.cn@gmail.com).

X. Wang is with the Electrical Engineering Department, Columbia University, New York, NY 10027, USA (e-mail: wangx@ee.columbia.edu).

tive for MIMO mechanisms than the detection error. [17], [18] propose model-based neural network architectures for sporadic user detection and channel estimation in massive machine-type communications. The deep unfolding framework is applied to design customized neural network layers through the unrolling of two iterative optimization algorithms. However, the ability of the networks to adapt to the potential mismatch between training or test data and signal models on which they are based is yet to be examined. Additionally, an algorithm is necessary to minimize the number of learnable parameters.

Millimeter wave massive MIMO is very important for 5G/6G wireless communication, that is, the number of paths is sparse compared to the number of base station antennas, this sparsity in mmWave channels can actually be better than the sparsity in user activity. In this paper, we propose several AMP algorithms to exploit the sparsity of mmWave channels for device activity detection and channel estimation.

C. Main Contributions

In this paper, we consider the problem of user activity detection and channel estimation in mmWave communication systems with massive MIMO, where the channel is a superposition of multiple complex sinusoids.

We setup the compressed sensing problem by exploiting two kinds of sparsities: 1) the user activity is sparse since only a fraction of devices are active; 2) the mmWave channel is sparse since the number of paths is usually much less than the number of BS antennas. To solve this compressed sensing problem, four methods are proposed based on AMP, on-grid approximation, soft-thresholding, hard-thresholding, atomic norm (AN) [19] and greedy techniques. Specifically, we extend the approach in [1] to the scenario of mmWave channel estimation. The mmWave channel exhibits two types of sparsity: channel sparsity and user activity sparsity. While [1] considers only one type of sparsity, our work models both types of sparsity simultaneously, providing a more comprehensive and innovative approach. In addition, the design of the denoisers in our framework is quite original, except for the first group-soft denoiser. Besides, the combination of the atomic norm with AMP is an innovative aspect of our work, which leads to a fast solver and it leads to significant performance improvements. Our main contributions are listed as follows.

1) A group soft-thresholding AMP is presented to exploit only the sparsity in user activity. Since in mmWave channel, the channel is not Rayleigh fading and the prior distribution may not be the Bernoulli Gaussian distribution [1]. The minimum mean-squared error (MMSE) denoiser does not apply. We hence take the group soft-thresholding function as the denoiser, which also has lower computationally load than the MMSE denoiser; 2) To further utilize the sparsity in the mmWave channel, we approximately define an overcomplete dictionary to construct the sparsity in mmWave channel. And then a hard-thresholding AMP is proposed based on the on-grid CS approach [20], [21]. Although the sparsity in mmWave channel is exploited, the frequencies in channel may not fall onto discrete grids [22]–[25] and hence hard-thresholding AMP suffers from performance loss; 3)

To overcome this difficulty, we exploit the atomic norm technique to address the off-grid problem to obtain super-resolution performance. Then, a direct SDP solver is proposed, which, however, has high computational complexity; 4) As a result, we finally combine the AMP and atomic norm techniques [19], [26]–[28] for user detection and channel estimation, which has moderate computational complexity. A greedy method is proposed as the super-resolution denoiser in the AMP, which includes the initialization, selection, local-optimization, least-squares and residual update steps.

In addition, the state evolution of the above proposed methods is analyzed. To ensure that the state evolution is accurate, we present methods for smoothing the denoisers to enable they are Lipschitz continuous [29]. In particular, the Monte Carlo sampling [30] is used to smooth the greedy denoiser and to calculate the derivative of the denoiser, which is required in the AMP iterations. And we prove that the derivative obtained by the Monte Carlo sampling is accurate as long as the number of Monte Carlo simulation goes to infinity. At last, simulation results show the advantage of the proposed methods for user activity detection and channel estimation in massive MIMO mmWave communication systems.

D. Organization

The remainder of the paper is organized as follows. We present the background in Section II. In Section III, we propose the group soft-thresholding AMP and the hard-thresholding AMP algorithms, and present the state evolution analysis results. In Section IV, we propose the SDP direct solver and the combined approach based on the AMP and atomic norm, which can overcome the off-grid problem. Besides, the smoothed denoiser is also presented. Simulation results are presented in Section V. Finally, Section VI concludes the paper.

II. BACKGROUND

A. Problem Formulation

Consider the uplink of a cellular network in which the base station is equipped with M antennas and contains N users each equipped with an antenna. Let $\mathbf{h}_n \in \mathbb{C}^{M \times 1}$ be the n -th user complex uplink channel vector to the BS. We adopt a block-fading model where \mathbf{h}_n remains constant within a coherence time block, and varies independently from block to block. For the mm-Wave channel [31], [32], \mathbf{h}_n can be modeled as

$$\mathbf{h}_n = \sum_{\ell=1}^{L_n} \bar{c}_{n,\ell} \mathbf{a}(f_{n,\ell}), \quad (1)$$

where $\bar{c}_{n,\ell} \in \mathbb{C}$ denotes the ℓ -th multipath gain; L_n denotes the number of paths; the vector $\mathbf{a}(f) \in \mathbb{C}^{M \times 1}$ denotes the steering responses of the receive array, given by

$$\mathbf{a}(f) = \frac{1}{\sqrt{M}} [1, e^{j2\pi f}, \dots, e^{j2\pi(M-1)f}]^T, \quad (2)$$

where $f = \frac{d \sin \theta}{2\lambda_w}$ with θ , d and λ_w denoting the angle of arrival, the separation of adjacent antenna elements and the wavelength of the transmitted signal, respectively.

Within each coherence block each user is active with probability ϵ . Denote

$$\alpha_n = \begin{cases} 1, & \text{if user } n \text{ is active,} \\ 0, & \text{otherwise,} \end{cases} \quad (3)$$

so that $\Pr(\alpha_n = 1) = \epsilon$, $\Pr(\alpha_n = 0) = 1 - \epsilon$.

Denote

$$\mathbf{u}_n = [u_{n,1}, u_{n,2}, \dots, u_{n,Q}]^T \in \mathbb{C}^{Q \times 1} \quad (4)$$

as the unique data symbols that is known by the BS.

Since we consider massive connection scenarios, the device number is usually greater than the length of the pilot sequence, i.e., $Q < N$. Therefore, it is impossible to assign mutually orthogonal sequences to all users.

Denote $\mathbf{Y} \in \mathbb{C}^{Q \times M}$ as the matrix of the received signal at the BS across M antennas over Q pilot symbols, given by

$$\mathbf{Y} = \sqrt{\rho} \sum_{n=1}^N \alpha_n \mathbf{u}_n \mathbf{h}_n^T + \mathbf{Z}, \quad (5)$$

where ρ is the pilot transmit power and the noise matrix $\mathbf{Z} \in \mathbb{C}^{Q \times M}$ contains i.i.d. $\mathcal{CN}(\mathbf{0}, \sigma_w^2)$ samples. Define

$$\mathbf{U} = [\mathbf{u}_1, \mathbf{u}_2, \dots, \mathbf{u}_N] \in \mathbb{C}^{Q \times N}, \quad (6)$$

$$\mathbf{X} = [\mathbf{x}_1, \mathbf{x}_2, \dots, \mathbf{x}_N]^T \in \mathbb{C}^{N \times M}, \quad (7)$$

where

$$\begin{aligned} \mathbf{x}_n &= \alpha_n \sqrt{\rho} \mathbf{h}_n = \alpha_n \sqrt{\rho} \sum_{\ell=1}^{L_n} \bar{c}_{n,\ell} \mathbf{a}(f_{n,\ell}) \\ &= \alpha_n \sum_{\ell=1}^{L_n} c_{n,\ell} \mathbf{a}(f_{n,\ell}) \end{aligned} \quad (8)$$

with $c_{n,\ell} = \sqrt{\rho} \bar{c}_{n,\ell}$. To simplify the notation, we let $\mathbf{h}_n = \sum_{\ell=1}^{L_n} c_{n,\ell} \mathbf{a}(f_{n,\ell})$ in the following. Then, (5) can be rewritten as

$$\mathbf{Y} = \mathbf{U} \mathbf{X} + \mathbf{Z}. \quad (9)$$

Our goal is to estimate the user activities (i.e., to obtain $\{\alpha_n\}$) and also to estimate the corresponding channels (i.e., to determine $\{\mathbf{h}_n : \alpha_n = 1\}$).

B. The AMP Solution and the Traditional Denoiser

Denote

$$\mathbf{X}^t = [\mathbf{x}_1^t, \dots, \mathbf{x}_N^t]^T \in \mathbb{C}^{N \times M}, \quad (10)$$

$$\mathbf{R}^t = [\mathbf{r}_1^t, \dots, \mathbf{r}_Q^t]^T \in \mathbb{C}^{Q \times M}, \quad (11)$$

as the estimate of \mathbf{X} and the corresponding residual at iteration t , respectively. By initializing to $\mathbf{X}^0 = \mathbf{0}$ and $\mathbf{R}^0 = \mathbf{Y}$, the vector AMP [33] algorithm is updated according to iterations:

$$\mathbf{x}_n^{t+1} = \eta_t((\mathbf{R}^t)^H \mathbf{u}_n + \mathbf{x}_n^t), \quad n = 1, 2, \dots, N, \quad (12)$$

$$\mathbf{R}^{t+1} = \mathbf{Y} - \mathbf{U} \mathbf{X}^{t+1} + \frac{1}{Q} \mathbf{R}^t \sum_{n=1}^N \eta_t'((\mathbf{R}^t)^H \mathbf{u}_n + \mathbf{x}_n^t), \quad (13)$$

where $\eta_t(\cdot) : \mathbb{C}^{M \times 1} \rightarrow \mathbb{C}^{M \times 1}$ is an appropriately designed non-linear function known as *denoiser* [34]–[37], and $\eta_t'(\cdot)$

is the first order derivative of $\eta_t(\cdot)$ with respect to the input argument.

In [1], the channel vector is modeled as an independent quasi-static flat fading component, i.e., \mathbf{h}_n in (1) is replaced by $\mathbf{h}_n \sim \mathcal{CN}(0, \beta_n \mathbf{I}_N)$ with β_n being the path-loss and shadowing component. Then, based on the conditional expectation, a MMSE denoiser is given by

$$\eta_t(\tilde{\mathbf{x}}_n^t) = \mathbb{E}(\mathbf{x}_n | \tilde{\mathbf{x}}_n^t) \quad (14)$$

with $\tilde{\mathbf{x}}_n^t = (\mathbf{R}^t)^H \mathbf{u}_n + \mathbf{x}_n^t$, which is specifically designed for the Rayleigh fading channel. For MMSE denoiser, once $\hat{\mathbf{X}}$ is obtained, the activity user can be detected and the channel can be estimated according to Definition 1 in [1].

However, in our case the channel is not Rayleigh fading and the prior distribution of \mathbf{x}_n may not be the Bernoulli Gaussian distribution [1]. Hence, the MMSE denoiser does not apply. Moreover, the MMSE denoiser can be computationally complex, so in practice some simplified form [36] or approximated denoiser [37] can be used instead.

III. PROPOSED ON-GRID SOLUTIONS BASED ON AMP

An effective approach for user detection and channel estimation is to exploit the sparsity of \mathbf{X} . Since \mathbf{x}_n 's are zero for those users are not active, \mathbf{X} is row sparse. Moreover, each \mathbf{x}_n is also sparse since there are sparse nature in \mathbf{h}_n , i.e., for the channel of mmWave communication, the number of paths is usually much smaller than the number of BS antennas, i.e., $L_n \ll M$ for $n = 1, 2, \dots, N$. In this section, we develop on-grid CS approaches based on the AMP algorithm by utilizing the user and channel sparsities.

A. Group Soft-thresholding AMP Based on User Activity Sparsity

Following [1], we use the vector AMP algorithm (12)–(13) for mmWave communication by exploiting the user sparsity. Once $\hat{\mathbf{X}}$ is obtained, we compare $\|\hat{\mathbf{x}}_n\|_1$ with a threshold ς to detect the activity users, i.e., a user is determined as activity if $\|\hat{\mathbf{x}}_n\|_1 > \varsigma$. The threshold ς is chosen to have a desired probabilities of miss detection and false alarm performance. Furthermore, when a device n is detected to be active, its channel is estimated to be $\hat{\mathbf{h}}_n = \hat{\mathbf{x}}_n$. Later, we will propose several denoisers that take advantage of both user sparsity and channel sparsity. Before that, we introduce another denoiser based on group soft-thresholding that only uses user sparsity, which is faster than MMSE denoiser in [1].

1) *Group soft-thresholding denoiser*: Since MMSE in [1] involves inversion operation, its computational complexity is $\mathcal{O}(M^3)$. To be more efficient, we estimate \mathbf{X} by formulating a group LASSO problem, i.e., we aim to find a group sparse $\hat{\mathbf{X}}$ that can minimize $\|\mathbf{Y} - \mathbf{U} \hat{\mathbf{X}}\|_F^2$ by solving

$$\hat{\mathbf{X}} = \arg \min_{\mathbf{X} \in \mathbb{C}^{N \times M}} \frac{1}{2} \|\mathbf{Y} - \mathbf{U} \mathbf{X}\|_F^2 + \gamma \|\mathbf{X}\|_{2,1}, \quad (15)$$

where $\|\mathbf{X}\|_{2,1} \triangleq \sum_{n=1}^N \|\mathbf{x}_n\|_2$, γ is the regularization parameter related to N , Q and \mathbf{X} . We use the vector AMP (12)–(13)

to solve (15), where it is straightforward to use the group soft-thresholding function as the denoiser. In particular, for any input $\tilde{\mathbf{x}}$ we have [38]

$$\begin{aligned}\eta_t^{\text{soft}}(\tilde{\mathbf{x}}) &= \arg \min_{\mathbf{x} \in \mathbb{C}^{M \times 1}} \frac{1}{2} \|\tilde{\mathbf{x}} - \mathbf{x}\|_2^2 + \lambda_t \|\mathbf{x}\|_2 \\ &= \frac{\tilde{\mathbf{x}}}{\|\tilde{\mathbf{x}}\|_2} (\|\tilde{\mathbf{x}}\|_2 - \lambda_t) \mathbb{I}(\|\tilde{\mathbf{x}}\|_2 \geq \lambda_t),\end{aligned}\quad (16)$$

where $\mathbb{I}(\cdot)$ denotes the indicator function. Obviously, the computational complexity of the group soft-thresholding denoiser is $\mathcal{O}(M)$, which is much smaller than that of the MMSE denoiser.

Note that for complex value function, the first order derivative $\eta'_t(\tilde{\mathbf{x}}) = \frac{\partial \eta_t(\tilde{\mathbf{x}})}{\partial \tilde{\mathbf{x}}}$ is calculated by

$$\begin{aligned}\frac{\partial \eta_t(\tilde{\mathbf{x}})}{\partial \tilde{\mathbf{x}}} &= \frac{1}{2} \left(\frac{\partial \eta_t(\tilde{\mathbf{x}})}{\partial \tilde{\mathbf{x}}^{\Re}} - i \frac{\partial \eta_t(\tilde{\mathbf{x}})}{\partial \tilde{\mathbf{x}}^{\Im}} \right) \\ &= \frac{1}{2} \left(\frac{\partial \eta_t^{\Re}(\tilde{\mathbf{x}})}{\partial \tilde{\mathbf{x}}^{\Re}} + \frac{\partial \eta_t^{\Im}(\tilde{\mathbf{x}})}{\partial \tilde{\mathbf{x}}^{\Im}} \right) \\ &\quad + \frac{i}{2} \left(\frac{\partial \eta_t^{\Re}(\tilde{\mathbf{x}})}{\partial \tilde{\mathbf{x}}^{\Im}} - \frac{\partial \eta_t^{\Im}(\tilde{\mathbf{x}})}{\partial \tilde{\mathbf{x}}^{\Re}} \right) \in \mathbb{C}^{M \times M},\end{aligned}\quad (17)$$

where $\eta_t^{\Re}(\cdot)$ and $\eta_t^{\Im}(\cdot)$ denote the real and imaginary parts, respectively; and $\tilde{\mathbf{x}}^{\Re}$ and $\tilde{\mathbf{x}}^{\Im}$ are the real and imaginary parts of the input $\tilde{\mathbf{x}} \in \mathbb{C}^{M \times 1}$, respectively. Hence, we have

$$\begin{aligned}\frac{\partial \eta_t^{\text{soft}}(\tilde{\mathbf{x}})}{\partial \tilde{\mathbf{x}}} &= \frac{\partial(\tilde{\mathbf{x}} - \lambda_t \tilde{\mathbf{x}} / \|\tilde{\mathbf{x}}\|_2)}{\partial \tilde{\mathbf{x}}} \mathbb{I}(\|\tilde{\mathbf{x}}\|_2 \geq \lambda_t) \\ &= \left[\mathbf{I}_M - \frac{\lambda_t}{2} \left(\frac{\partial \frac{\tilde{\mathbf{x}}^{\Re} + i \tilde{\mathbf{x}}^{\Im}}{\|\tilde{\mathbf{x}}\|_2}}{\partial \tilde{\mathbf{x}}^{\Re}} - i \frac{\partial \frac{\tilde{\mathbf{x}}^{\Re} + i \tilde{\mathbf{x}}^{\Im}}{\|\tilde{\mathbf{x}}\|_2}}{\partial \tilde{\mathbf{x}}^{\Im}} \right) \right] \mathbb{I}(\|\tilde{\mathbf{x}}\|_2 \geq \lambda_t) \\ &= \left[\mathbf{I}_M - \frac{\lambda_t}{\|\tilde{\mathbf{x}}\|_2} \mathbf{I}_M + \lambda_t \frac{\tilde{\mathbf{x}} \tilde{\mathbf{x}}^H}{2 \|\tilde{\mathbf{x}}\|_2^3} \right] \mathbb{I}(\|\tilde{\mathbf{x}}\|_2 \geq \lambda_t).\end{aligned}\quad (18)$$

In practice, it is convenient to set $\lambda_t = \tau \sigma_t$ in which τ is a constant and $\sigma_t = \frac{1}{\sqrt{MQ}} \|\mathbf{R}^t\|_F$ [38]. In this paper, we name the AMP with the group soft-thresholding as GST-AMP.

2) *State evolution*: Note that since the ground truth \mathbf{X}^* is unknown, we cannot directly calculate $\|\hat{\mathbf{X}} - \mathbf{X}^*\|_2^2$ to obtain the estimation performance of (12)-(13) against the iteration number. Alternatively, we calculate the state evolution to predict the estimation performance in certain asymptotic regime. A remarkable property of the AMP algorithm is that when applied to the compressed sensing problem with the entries of the sensing matrix \mathbf{U} generated from i.i.d. Gaussian distribution, its estimation performance in certain asymptotic regime can be accurately predicted by the so-called state evolution. In particular, when $Q, K, N \rightarrow \infty$ (K is the active users) the ratios converge to positive constants, i.e., $K/N \rightarrow \epsilon$ and $Q/N \rightarrow \omega$.

Denote $\Theta_0 = \frac{1}{N} \sum_{n=1}^N \mathbf{x}_n \mathbf{x}_n^H$, then a series of state evolution matrices are generated by the following iterations:

$$\begin{aligned}\Theta_{t+1}(\mathbf{X}, \sigma_w^2) &= \frac{1}{N} \sum_{n=1}^N \mathbb{E} \left[\left(\eta_{t+1} \left(\mathbf{x}_n + \Sigma_t^{1/2} \mathbf{v}_n \right) - \mathbf{x}_n \right) \right. \\ &\quad \left. \left(\eta_{t+1} \left(\mathbf{x}_n + \Sigma_t^{1/2} \mathbf{v}_n \right) - \mathbf{x}_n \right)^H \right].\end{aligned}\quad (19)$$

where the expectation is with respect to $\mathbf{v}_n \sim \mathcal{CN}(\mathbf{0}, \mathbf{I}_M)$ for $n = 1, 2, \dots, N$; recall that σ_w^2 is the variance of the noise; $\eta_t(\cdot)$ is the same as (16) with λ_t replaced by $\bar{\lambda}_t = \tau \sqrt{\text{Tr}(\Sigma_t)}$, where $\text{Tr}(\cdot)$ is the trace of the input matrix; and

$$\Sigma_t = \frac{1}{\omega} \Theta_t(\mathbf{X}, \sigma_w^2) + \sigma_w^2 \mathbf{I}_M \quad (20)$$

is referred to as the state. Based on the standard state evolution analysis (e.g. Theorem 1 in [34] and Theorem 1 in [35]) when Q and N are large enough, the state evolution can predict the MSE of the algorithm, i.e.,

$$\Theta_{t+1}(\mathbf{X}, \sigma_w^2) \approx \frac{1}{N} \sum_{n=1}^N (\mathbf{x}_n^{t+1} - \mathbf{x}_n)(\mathbf{x}_n^{t+1} - \mathbf{x}_n)^H. \quad (21)$$

The above equations give a general framework to analyze the performance of the AMP. Obviously, the smaller $\text{Tr}(\Theta_{t+1}(\mathbf{X}, \sigma_w^2))$ is, the smaller the reconstruction error will be.

B. Hard-thresholding AMP Based on Channel Sparsity

The GST-AMP exploits the sparsity in the user activity pattern, but does not use the sparsity of the mmWave channel. We next propose a new method Hard-thresholding AMP that can exploit these two sparsity. Recall that the channel is sparse in spatial domain, i.e., L_n is small compared to M . For better user detection and channel estimation, the channel sparsity is investigated and an improved AMP is proposed with a different $\eta_t(\cdot)$. Define an overcomplete dictionary

$$\mathbf{A} = [\mathbf{a}(f'_1), \mathbf{a}(f'_2), \dots, \mathbf{a}(f'_{\tilde{M}})] \in \mathbb{C}^{M \times \tilde{M}}, \quad (22)$$

where $\{f'_m\}$ is sets of uniformly spaced frequency points and $\tilde{M} > M$ is the number of grid points. If the frequencies $\{f_{n,\ell}\}_{1 \leq \ell \leq L_n}$ in (1) fall on the grids for $n = 1, 2, \dots, N$, let $\tilde{\mathbf{c}}_n$ be the corresponding L_n -sparse coefficient vector, i.e., $\mathbf{h}_n = \mathbf{A} \tilde{\mathbf{c}}_n$ and $\|\tilde{\mathbf{c}}_n\|_0 = L_n$, then we have $\mathbf{A}^H \mathbf{h}_n = \mathbf{A}^H \mathbf{A} \tilde{\mathbf{c}}_n = \tilde{\mathbf{c}}_n$ is L_n -sparse. Further, we have $\mathbf{A}^H \mathbf{x}$ is L_n -sparse or 0-sparse when $\alpha_n = 0$. Hence, to enhance the performance of channel estimation, we denoise $\tilde{\mathbf{x}}$ by solving

$$\arg \min_{\mathbf{x}} \|\mathbf{A}^H \mathbf{x}\|_1, \text{ s.t. } \|\mathbf{x} - \tilde{\mathbf{x}}\|_2^2 \leq \gamma, \quad (23)$$

where γ is a threshold that can be adaptively changed in each iteration. (23) introduces a way to exploit the sparsity of \mathbf{x} . It is known that we can use a hard-thresholding function as the denoiser to solve (23), for any input $\tilde{\mathbf{x}}$ we have

$$\eta_t^{\text{hard}}(\tilde{\mathbf{x}}) = \mathbf{A} \mathbb{V}(\mathbf{A}^H \tilde{\mathbf{x}}), \quad (24)$$

where $\mathbb{V}(\mathbf{v}) = [\mathbb{V}(v_1), \mathbb{V}(v_2), \dots, \mathbb{V}(v_{\tilde{M}})]^T$ with $\mathbf{v} \in \mathbb{C}^{\tilde{M} \times 1}$ and $\mathbb{V}(v_m) = v_m \mathbb{I}(|v_m| > \lambda_t)$. In addition, we have

$$\frac{\partial \eta_t^{\text{hard}}(\tilde{\mathbf{x}})}{\partial \tilde{\mathbf{x}}} = \frac{\partial (\mathbf{A} \mathbb{V}(\mathbf{A}^H \tilde{\mathbf{x}}))}{\partial \tilde{\mathbf{x}}} = \mathbf{A} \text{diag}(\bar{\mathbb{V}}(\mathbf{A}^H \tilde{\mathbf{x}})) \mathbf{A}^H, \quad (25)$$

where $\text{diag}(\cdot)$ denotes the diagonal operator, whose output is an diagonal matrix with diagonal entries are the input vector; $\bar{\mathbb{V}}(\mathbf{v}) = [\bar{\mathbb{V}}(v_1), \bar{\mathbb{V}}(v_2), \dots, \bar{\mathbb{V}}(v_{\tilde{M}})]^T$ with $\mathbf{v} \in \mathbb{C}^{\tilde{M} \times 1}$ and $\bar{\mathbb{V}}(v_m) = \mathbb{I}(|v_m| > \lambda_t)$. In this paper, we name the AMP

with the hard-thresholding as HT-AMP. Based on (23) and (9), the algorithm provides the solution to

$$\begin{aligned} \{\hat{\mathbf{x}}_n\}_{n=1}^N &= \arg \min_{\{\mathbf{x}_n\}_{n=1}^N} \sum_{n=1}^N \|\mathbf{A}^H \mathbf{x}_n\|_1, \\ \text{s.t. } &\left\| \mathbf{Y} - \sum_{n=1}^N \mathbf{u}_n \mathbf{x}_n^T \right\|_F \leq \zeta, \end{aligned} \quad (26)$$

where $\zeta > 0$ is a weight factor. The objective in (26) can be understood as we first utilize the ℓ_1 -norm $\|\mathbf{A}^H \mathbf{x}_n\|_1 = \|\alpha_n \tilde{\mathbf{c}}_n\|_1$ to exploit the channel sparsity, then use $\sum_{n=1}^N$ to exploit the user sparsity since $\sum_{n=1}^N \|\alpha_n \tilde{\mathbf{c}}_n\|_1 = \left\| \left[\|\alpha_1 \tilde{\mathbf{c}}_1\|_1, \dots, \|\alpha_N \tilde{\mathbf{c}}_N\|_1 \right]^T \right\|_1$.

The denoiser used within AMP can take on almost any form, and the SE of the HT-AMP can be obtained via (19)-(21) with $\eta(\cdot)$ function in (19) replaced by (24). However, the denoiser needs to be Lipschitz continuous [29], otherwise the SE prediction is not accurate enough. One simple idea is to “smooth” the denoisers. In particular, we can decompose $\mathbb{V}(v)$ to [34]

$$\mathbb{V}(v) = S_t(v) + D_t(v), \quad (27)$$

where $S_t(v)$ is a weakly differentiable function and can be set as the Lipschitz continuous function of v , while $D_t(v)$ is a piece-wise constant function and is not continuous. Then, we introduce the Gaussian kernel, denoted by $G_\varepsilon(v)$, where the standard deviation is $\varepsilon > 0$. In this way, we have the following smoothed denoiser [34]

$$\tilde{\mathbb{V}}(v) = S_t(v) + D_t(v) * G_\varepsilon(v), \quad (28)$$

where $*$ denotes the convolution operator. By using the smoothed denoiser, we can obtain the accurate state evolution of the HT-AMP. We refer the reader to [34] for more details of the smoothed denoiser. Alternatively, one can smooth the denoiser according to Monte Carlo sampling [30], which is similar to the method introduced in the next section, hence the details are omitted here for simplicity.

Note that the frequencies in the channel signal \mathbf{h}_n are in continuous space. Hence the on-grid CS approach HT-AMP used here yields performance loss. In the next section, we introduce the off-grid CS approach based on atomic norm and super resolution AMP to solve this problem.

IV. PROPOSED OFF-GRID SOLUTIONS BASED ON AMP & ATOMIC NORM

In this section, we introduce AN techniques to model the sparse representation to achieve the super-resolution performance. Then we propose super resolution AMP based on greedy denoiser by exploiting the sparsity in mmWave channel.

A. Towards Super Resolution Solver Based on Atomic Norm

We investigate better denoiser for the channel estimation. Notice that for the channel of mmWave communication, the number of paths is usually much smaller than the number of BS antennas, i.e., $L_n \ll M$ for $n = 1, 2, \dots, N$. Hence, there

are also sparse nature in \mathbf{h}_n . However, the channel signal \mathbf{h}_n is a linear combination of complex sinusoids, the phase of which is arbitrary, i.e. in continuous space. Therefore, using ℓ_1 -norm to construct a sparse representation must place the frequencies onto discrete grids. Obviously, this step will introduce errors. To get rid of the grid operation, we use the atomic norm to achieve off-grid property.

Define $\mathbf{a}(f)$ as an atom and $\mathcal{A} = \{\mathbf{a}(f) : f \in [0, 1]\}$ as the atom set. $\mathbf{x}_n = \alpha_n \sum_{\ell=1}^{L_n} c_{n,\ell} \mathbf{a}(f_{n,\ell})$ in (8) can be regarded as $\mathbf{x}_n = \sum_{\ell=1}^{L_n} c_{n,\ell} \mathbf{a}(f_{n,\ell})$ with $c_{n,\ell} = \sqrt{\rho} \tilde{c}_{n,\ell}$ when user is active and $c_{n,\ell} = 0$ otherwise. Then, the ℓ_p -atomic norm related to (8) is defined as follows.

Definition 1. The ℓ_p -atomic norm for $\mathbf{x} \in \mathbb{C}^{M \times 1}$ is

$$\|\mathbf{x}\|_{\mathcal{A},p} = \inf_{\substack{f_\ell \in [0,1] \\ c_\ell \in \mathbb{C}}} \left\{ \left(\sum_{\ell} |c_\ell|^p \right)^{1/p} \middle| \mathbf{x} = \sum_{\ell} c_\ell \mathbf{a}(f_\ell) \right\}. \quad (29)$$

The ℓ_p -atomic norm can enforce sparsity in the atom set \mathcal{A} . Then, we can formulate the following optimization problem according to (9)

$$\begin{aligned} \{\hat{\mathbf{x}}_n\}_{n=1}^N &= \arg \min_{\{\mathbf{x}_n\}_{n=1}^N} \sum_{n=1}^N \|\mathbf{x}_n\|_{\mathcal{A},p}, \\ \text{s.t. } &\left\| \mathbf{Y} - \sum_{n=1}^N \mathbf{u}_n \mathbf{x}_n^T \right\|_F \leq \zeta, \end{aligned} \quad (30)$$

where $\zeta > 0$ is a weight factor. However, (30) cannot be directly solved because the ℓ_p -atomic norm is essentially a semi-infinite program. In the next section, we propose the super resolution AMP for solving (30). Before that, we introduce a way to solve this problem when $p = 1$ so that we can better understand it.

In the case of $p = 1$, we can use the equivalent form of the atomic norm for the atom set \mathcal{A} [19] to solve (30). Specifically, we have

$$\|\mathbf{x}\|_{\mathcal{A},1} = \inf_{\mathbf{v} \in \mathbb{C}^{M \times 1}, t \in \mathbb{R}} \left\{ \frac{1}{2M} \text{Tr}(\text{Toep}(\mathbf{v})) + \frac{t}{2}, \text{ s.t. } \begin{bmatrix} \text{Toep}(\mathbf{v}) & \mathbf{x} \\ \mathbf{x}^H & t \end{bmatrix} \succeq 0 \right\}, \quad (31)$$

where $\text{Toep}(\cdot)$ denotes the Hermitian Toeplitz matrix whose first column is the input vector, i.e.,

$$\text{Toep}(\mathbf{v}) = \begin{bmatrix} v_1 & v_2^* & \cdots & v_M^* \\ v_2 & v_1 & \cdots & v_{M-1}^* \\ \vdots & \vdots & \ddots & \vdots \\ v_M & v_{M-1} & \cdots & v_1 \end{bmatrix}. \quad (32)$$

The relationship of (31) and (32) is given by

$$\text{Toep}(\mathbf{v}) = \sum_{\ell} |c_\ell| \mathbf{a}(f_\ell) \mathbf{a}(f_\ell)^H, \quad (33)$$

$$t = \sum_{\ell} |c_\ell|. \quad (34)$$

Then, we can apply (31) and transform (30) to the following

semidefinite program (SDP):

$$\begin{aligned} \{\hat{\mathbf{x}}_n\}_{n=1}^N = & \arg \min_{\{\mathbf{x}_n, \mathbf{v}_n, t_n\}_{n=1}^N} \frac{\zeta}{2M} \sum_{n=1}^N \text{Tr}(\text{Toep}(\mathbf{v}_n)) + \sum_{n=1}^N \frac{\zeta t_n}{2}, \\ \text{s.t.} & \left\| \mathbf{Y} - \sum_{n=1}^N \mathbf{u}_n \mathbf{x}_n^T \right\|_F \leq \zeta, \\ & \begin{bmatrix} \text{Toep}(\mathbf{v}_n) & \mathbf{x}_n \\ \mathbf{x}_n^H & t_n \end{bmatrix} \succeq 0, \quad n = 1, 2, \dots, N. \end{aligned} \quad (35)$$

The above SDP problem can be solved by CVX [39], SeDuMi [40], SDPT3 [41] and any other convex solvers. However, these solver tend to be slow as the size of the problem becomes large. In addition, in the case of $p = 0$, the problem (30) is non-convex, so cannot be solved with a convex solver. Hence, we next propose the super-resolution AMP with faster speed.

B. Super-Resolution AMP Based on Greedy Denoiser

1) *Greedy denoiser and its smooth form:* We combine the atomic norm optimization with the framework of AMP to solve (30), i.e., the AMP algorithm uses the atomic norm-based denoiser in each iteration. We call such AMP algorithm that employs a super-resolution denoiser as S-AMP. For clarity, we come back to the 1D-array case and denote the super-resolution denoiser as $\eta_t(\cdot)$ which can be applied to $\tilde{\mathbf{x}} = \mathbf{x} + \Sigma_t^{1/2} \mathbf{v}$ with $\mathbf{v} \sim \mathcal{CN}(\mathbf{0}, \mathbf{I}_M)$ and will return an estimate of \mathbf{x} that is hopefully closer to $\mathbf{x} + \Sigma_t^{1/2} \mathbf{v}$. S-AMP assumes that \mathbf{x}_n is sparse in continuous frequency domain. Suppose we use the denoiser

$$\begin{aligned} \eta_t(\tilde{\mathbf{x}}) = & \arg \min_{\mathbf{x} \in \mathbb{C}^{M \times 1}} \|\mathbf{x}\|_{\mathcal{A}, p}, \\ \text{s.t.} & \|\tilde{\mathbf{x}} - \mathbf{x}\|_2 \leq \gamma, \end{aligned} \quad (36)$$

where γ is a threshold that can be adaptively changed in each iteration. The algorithm can obtain the estimate of \mathbf{X} via iterating (12) and (13). Note that (36) is non-convex and its global optimum may not be obtained in polynomial time. Specifically, inspired by recent work on atomic norm minimization based on the conditional-gradient method [42], [43], we adopt the following procedure as the denoiser in the case of $p = 0$, which includes the initialization, selection, local-optimization, least-squares and residual update steps. The iterative process is below and the detail is in VI-C Super-resolution AMP (S-AMP)

The greedy denoiser in steps 1) to 5) can be directly used in AMP iterations (12) and (13). However, as mentioned above, we also need to smooth the greedy denoiser, i.e., find a smooth version that without discontinuities and behave almost the same as the original noise reducer, so as to satisfy the state evolution equations. Suppose $\eta_t(\cdot)$ is discontinuous. The smoothed denoiser can be obtained via [29]

$$\tilde{\eta}_t(\tilde{\mathbf{x}}) = \int_{\zeta \in \mathbb{C}^{M \times 1}} \eta_t(\tilde{\mathbf{x}} - \zeta) \frac{1}{r^M (2\pi)^{M/2}} e^{-\|\zeta\|_2^2 / 2r^2} d\zeta, \quad (37)$$

where $d\zeta = d\zeta_1 d\zeta_2 \dots d\zeta_M$.

Since (37) integrates over $\mathbb{C}^{M \times 1}$ based on the unknown form $\eta_t(\cdot)$, we calculate this via Monte Carlo sampling [30]. First we randomly generated some complex Gaussian vectors

Algorithm 1 Super-resolution AMP (S-AMP)

Require: Observation vector $\tilde{\mathbf{x}}$, Maximum iterations I, I' , Step size

μ_i , Stopping criteria ϵ, δ , Thresholds $\gamma, \tilde{\delta}$

Ensure: Estimated spectral lines \mathcal{T}

1: **Initialization:**

2: $\mathcal{T} \leftarrow \emptyset$

3: $\mathbf{r}_{\text{res}} \leftarrow \tilde{\mathbf{x}}$

4: **repeat**

5: **Selection:**

6: Compute highest correlated atom f°

7: Update $\mathcal{T} : \mathcal{T} \leftarrow \mathcal{T} \cup \{f^\circ\}$

8: **Local optimization:**

9: Define \mathbf{c} and \mathbf{f} using \mathcal{T}

10: Refine \mathbf{f} by solving the optimization problem

11: Calculate gradient and Hessian matrix

12: Update \mathbf{f} using Newton's method: $\mathbf{f}^{i+1} = \mathbf{f}^i - \mu_i \mathbf{K}(\mathbf{f}^i)^{-1} \mathbf{p}(\mathbf{f}^i)$

13: **Least-squares:**

14: Estimate \mathbf{c} by solving the least-squares problem

15: Remove any atoms in \mathcal{T} with coefficients smaller than $\tilde{\delta}$

16: **Residual update:**

17: $\mathbf{r}_{\text{res}} = \tilde{\mathbf{x}} - \Phi(\hat{\mathbf{f}}) \hat{\mathbf{c}}$

18: **until** $\|\mathbf{r}_{\text{res}}\|_2^2 \leq \epsilon$ or maximum iteration number I' is reached

$\mathbf{b}^1, \mathbf{b}^2, \dots, \mathbf{b}^{J_1}$ with standard deviation r . Then, we smooth the denoiser by

$$\hat{\eta}_t(\tilde{\mathbf{x}}) = \frac{1}{J_1} \sum_{j=1}^{J_1} \eta_t(\tilde{\mathbf{x}} + \mathbf{b}^j), \quad (38)$$

where $\mathbf{b}^j \sim \mathcal{CN}(\mathbf{0}, r^2 \mathbf{I}_M)$ for all j . As a result, \mathbf{x}_n^{t+1} can be updated via (12) with $\eta_t(\cdot)$ replaced by the smooth greedy denoiser $\hat{\eta}_t(\cdot)$. In addition, the SE of S-AMP can be obtained via (19)-(21) with the eta function in (19) replaced by (38).

2) *Derivative:* To perform the AMP iterations in (12) and (13), $\sum_{n=1}^N \frac{\partial \hat{\eta}_t}{\partial \tilde{\mathbf{x}}}(\tilde{\mathbf{x}}_n^t)$ should also be calculated. However, this is difficult since we do not have access to the explicit form of the greedy denoiser $\eta_t(\cdot)$. To solve this problem, we also calculate $\sum_{n=1}^N \frac{\partial \hat{\eta}_t}{\partial \tilde{\mathbf{x}}}(\tilde{\mathbf{x}}_n^t)$ by using the Monte Carlo simulation [30]. That is, for $1 \leq m \leq M$ and $1 \leq n \leq N$, we first generate J_2 vectors $\mathbf{d}_{m,n}^1, \mathbf{d}_{m,n}^2, \dots, \mathbf{d}_{m,n}^{J_2}$ whose m -th element obeys i.i.d. complex Gaussian distribution $\mathcal{CN}(0, 1)$ and the rest of the elements are zero.

Next, define

$$\mathbf{v}_m \triangleq \sum_{n=1}^N \frac{\partial \hat{\eta}_t(\tilde{\mathbf{x}}_n)}{\partial \tilde{\mathbf{x}}_n(m)} \in \mathbb{C}^{M \times 1}. \quad (39)$$

Then, from the following Theorem 1, (the proof process is in Section VI-B), we can find that for large J_1, J_2 and for very small ϵ , \mathbf{v}_m can be approximately obtained by averaging

$$\mathbf{v}_m \approx \frac{1}{J_2} \sum_{k=1}^{J_2} \mathbf{v}_{m,k}, \quad (40)$$

where

$$\begin{aligned} \mathbf{v}_{m,k} &= \sum_{n=1}^N \frac{d_{m,n}^k(m)}{\varepsilon} \left(\hat{\eta}_t(\tilde{\mathbf{x}}_n + \varepsilon \mathbf{d}_{m,n}^k) - \hat{\eta}_t(\tilde{\mathbf{x}}_n) \right) \\ &= \sum_{n=1}^N \frac{d_{m,n}^k(m)}{\varepsilon J_1} \sum_{j=1}^{J_1} \left(\eta_t(\tilde{\mathbf{x}}_n + \mathbf{b}^j + \varepsilon \mathbf{d}_m^k) - \eta_t(\tilde{\mathbf{x}}_n + \mathbf{b}^j) \right), \end{aligned} \quad (41)$$

where $d_{m,n}^k(m)$ is the m -th element of $\mathbf{d}_{m,n}^k$.

C. Computational Complexity Analysis

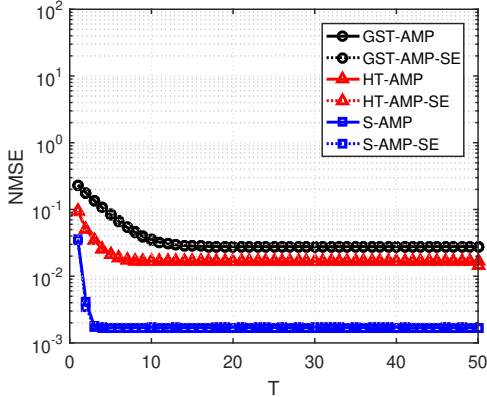


Fig. 1: Convergence behaviors of the proposed detectors and their state evolutions.

In this section, we analyze the computational complexity of the proposed methods in the Table I. In addition to the denoiser, the complexity of the AMP iterations in (12) and (13) mainly comes from $\mathbf{U}\mathbf{X}^{t+1}$, which is $\mathcal{O}(QNM)$ per iteration. For the denoisers, the computational complexity of the group soft-thresholding denoiser in (16) is $\mathcal{O}(M)$, which is smaller than that of the MMSE denoiser ($\mathcal{O}(M^3)$) in [1]. In addition, the computational complexities of the hard-thresholding denoiser in (24) and (25) are respectively $\mathcal{O}(MM)$ and $\mathcal{O}(M^2M)$. As for the SDP problem, if it is solved by the interior point method, the complexity is $\mathcal{O}(M^6N)$ per iteration [24], [44]. The main complexity of the greedy denoiser comes from (51) and (52), with respectively complexities $\mathcal{O}(M^3)$ and $\mathcal{O}(M^2|\mathcal{T}|)$ per inner iteration (we named the iterations of steps 1)-5) in the greedy denoiser as the inner iterations to distinguish them from the AMP iterations). Since $M < N$ and $M < Q$, the computational complexities of GST-AMP, HT-AMP, SDP and S-AMP methods are $\mathcal{O}(QNM)$, $\mathcal{O}(QNM)$, $\mathcal{O}(M^6N)$ and $\mathcal{O}(QNM)$, respectively.

V. SIMULATIONS

A. Simulation Setup

In this section, we present the numerical simulation examples to demonstrate the performance of the proposed algorithms. In addition to the parameters specified in the following simulations, the basic parameters are set as follows, the number of devices in the cell is set as $N = 2000$.

TABLE I: Comparison of Computational Complexities

Method	Complexity
AMP iterations	$\mathcal{O}(QNM)$
Group soft-thresholding denoiser	$\mathcal{O}(M)$
MMSE denoiser [1]	$\mathcal{O}(M^3)$
Hard-thresholding denoiser	$\mathcal{O}(MM)$
SDP (interior point method) [24], [44]	$\mathcal{O}(M^6N)$
Greedy denoiser (gradient)	$\mathcal{O}(M^3)$
Greedy denoiser (Hessian)	$\mathcal{O}(M^2 \mathcal{T})$
GST-AMP	$\mathcal{O}(QNM)$
HT-AMP	$\mathcal{O}(QNM)$
S-AMP	$\mathcal{O}(QNM)$

We set the probability $\epsilon = 0.05$ and hence the active user number (pilot sequence) is $K = 100$. A quadrature phase-shift keying (QPSK) modulation is used for pilot sequence [25]. Note that in the following simulations, we assume that each user has a unique pilot sequence to be consistent with the method in [1], [17] for a fair comparison. The complex multi-path gains $c_{n,\ell}$ in (1) are set as $c_{n,\ell} \sim \mathcal{CN}(0, 1)$, and the antenna number $M = 32$. The communication system uses a signal with $Q = 1000$ data symbols, and a total bandwidth of 100 MHz, i.e., the frequency spacing between adjacent subcarriers is 100 kHz. The transmit power of the active users is $\rho^{\text{pilot}} = 30$ dBm. The power spectral density of the AWGN at the BS is set as -174 dBm/Hz with a -94 dB pathloss.

To evaluate the performance achieved by the proposed detectors, we follow the same way in [1] to calculate the missed detection and false alarm to evaluate the proposed detectors. We invite readers to refer to [1] for more details. Besides, we calculate the normalized mean-squared-error (NMSE) $\|\hat{\mathbf{X}} - \mathbf{X}\|_F / \|\mathbf{X}\|_F$ to evaluate the proposed detectors. In the following simulations, we compare the performance of the proposed GST-AMP, HT-AMP and S-AMP detectors with the MMSE-AMP detector in [1] and MMSE-NET detector in [17]. However, the proposed SDP detector is not included in the comparison because its computational complexity is 5 orders of magnitude higher than other proposed detectors, which is analyzed at the end of Section IV. Moreover, we calculate the state evolution of the proposed GST-AMP, HT-AMP and S-AMP detectors, which are respectively named GST-AMP-SE, HT-AMP-SE and S-AMP-SE. All performance curves of GST-AMP, HT-AMP, MMSE-AMP and MMSE-NET detectors are averaged results after at least 20000 runs, while those of S-AMP detector are averaged results after at least 2000 runs.

B. Simulation Results

1) *Convergence behavior*: The convergence behavior is analyzed in Fig. 1. The NMSE in each iteration is calculated, we can see that HT-AMP and S-AMP detectors can converge within 10 iterations, while GST-AMP detector can converge within 15 iterations. Therefore, in subsequent simulations, we let the detectors iterate until the difference between the two updates is less than $\epsilon = 10^{-6}$, or iterate until reach the maximum number of iterations, which is set to 10 for HT-AMP and S-AMP detectors, and 15 for GST-AMP detector. In addition, we can see that the state evolution curves GST-AMP-SE, HT-AMP-SE and S-AMP-SE coincide with the

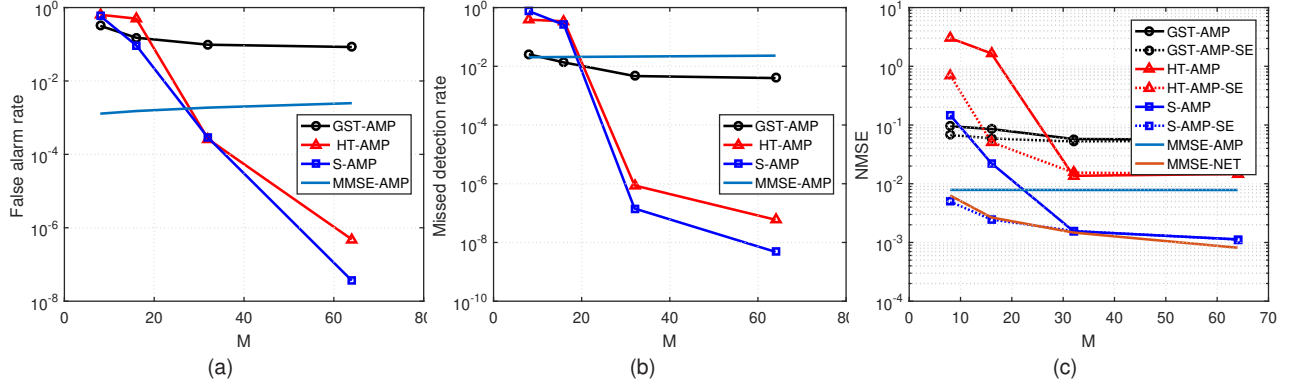


Fig. 2: Numerical simulation results against the number of antennas (M) at the BS. (a) False alarm; (b) Missed detection; (c) NMSE and state evolution.

NMSE curves of GST-AMP, HT-AMP and S-AMP detectors, respectively.

2) *Simulation results under different M* : Fig. 2(a) and (b) respectively show the false alarm and missed detection versus M , i.e., the number of antennas at the BS. Fig. 2(c) shows the NMSE of \mathbf{X} in (7) versus M . We can see that when M increases, the performance of the proposed HT-AMP and S-AMP detectors will be significantly better. This is because when M increases, the sparsity of the millimeter wave channel becomes better. In contrast, the MMSE-AMP detector in [1] and the proposed GST-AMP detector do not exploit the sparsity of the mmWave channel, so the performance does not change much, as the number of antennas M increases, the number of groups also increases, and each group becomes smaller in size. This results in a decrease in the sparsity of each group, which in turn affects the performance of the GST-AMP. And the GST-AMP performance is worse than that of HT-AMP and S-AMP detectors for large M .

Moreover, compared to S-AMP detector, the on-grid based HT-AMP detector suffers performance loss, since the frequencies do not fall onto discrete grids and S-AMP detector can obtain more accurate channel frequencies. Note that although the NMSE of the MMSE-AMP detector is relatively small, its false alarm and missed detection rate are higher than that of the HT-AMP detector for large M . This is because the HT-AMP detector is less likely to fail, but when it fails, it may produce a larger error NMSE, which will result in a higher average value. Furthermore, we can see that when M is large enough, the state evolution curves GST-AMP-SE, HT-AMP-SE and S-AMP-SE coincide with the NMSE curves of GST-AMP, HT-AMP and S-AMP detectors, respectively, while there is a gap between them when M is small since the detectors may have error under non-sparse conditions.

3) *Simulation results under different K* : Figs. 3(a) and (b) show the false alarm and missed detection versus the numbers of active users K , respectively. Fig. 3(c) shows the NMSE of \mathbf{X} versus K . We can see that the proposed HT-AMP and S-AMP detectors can achieve better performance than the MMSE-AMP detector and the proposed GST-AMP detector, since they further exploit the sparsity of the mmWave channel. In addition, we can see that when K becomes larger,

the sparsity in the user activity pattern will be worse. Hence, all detectors have performance losses in terms of NMSE, false alarm and missed detection rates, except for GST-AMP detector where the false alarm rate becomes better. This may be due to the lack of stability of the group soft-thresholding denoiser, i.e., there will be some erroneous estimates which lead to deviations in the average value, but when K becomes larger, the wrong estimate is more likely to be included in the correct result. Another possible reason is due to an insufficient number of samples used in our experiments. Consequently, the initial random seeds used for generating values may have a relatively significant impact on the false alarm rate.

4) *Simulation results under different Q* : Figs. 4(a) and (b) show the false alarm and missed detection versus the length of data symbols Q , respectively. Fig. 4(c) shows the NMSE of \mathbf{X} versus Q . We can see that the proposed HT-AMP and S-AMP detectors can achieve better performance than the MMSE-AMP detector and the proposed GST-AMP detector. In addition, when Q becomes larger, the performance of the proposed detectors become better, since the sparsity condition becomes better. Moreover, we can see that when Q is large enough, the state evolution curves GST-AMP-SE, HT-AMP-SE and S-AMP-SE coincide with the NMSE curves of GST-AMP, HT-AMP and S-AMP detectors, respectively, while there is a gap between them when Q is small since the detectors may have error under non-sparse conditions.

5) *Simulation results under different SNR*: Figs. 5(a) and (b) show the false alarm and missed detection versus source SNR, respectively. Fig. 5(c) shows the NMSE of \mathbf{X} versus SNR. With the SNR increases, all detectors have performance improvement in terms of NMSE, false alarm and missed detection rates, except for GST-AMP and MMSE detectors where the false alarm rate may increase. This phenomenon also appears in Fig. 3, which may be caused by a trade-off between the false alarm and missed detection rates. When the missed detection rate drops a lot, it shows that we are more inclined to regard noise as the target, and the false alarm rate increases instead. Another possible reason is due to the limited number of samples used in our experiments, the false alarm rate was impacted by false signals at specific conditions, particularly

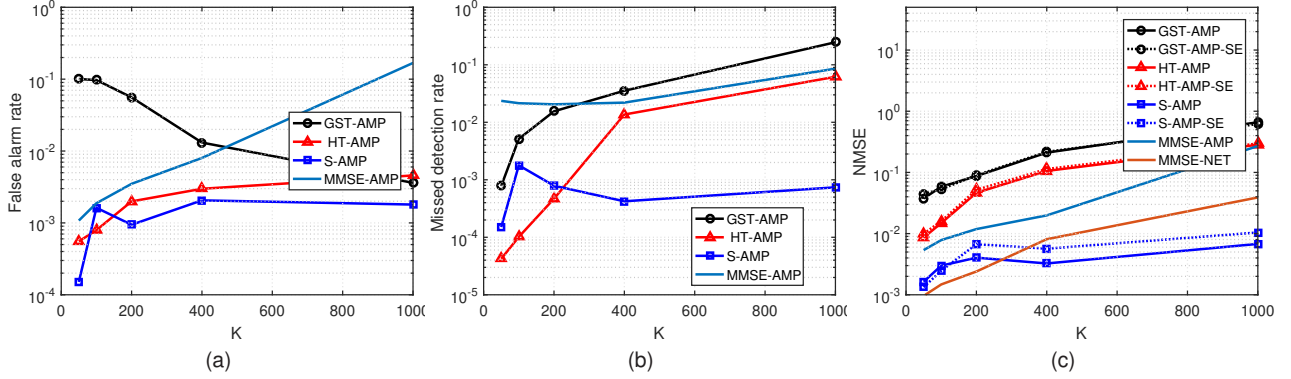


Fig. 3: Numerical simulation results as functions of the number of active users (K). (a) False alarm; (b) Missed detection; (c) NMSE and SE.

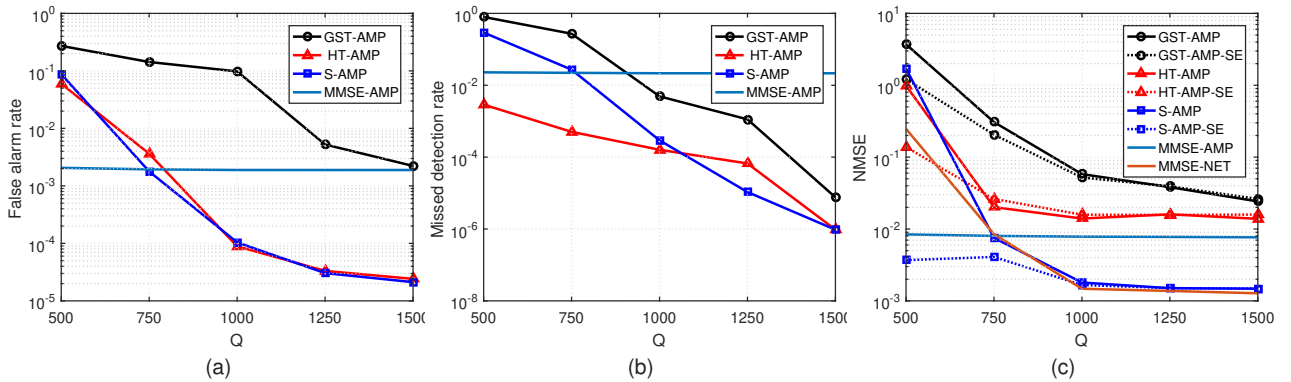


Fig. 4: Numerical simulation results as functions of the length of data symbols (Q). (a) False alarm; (b) Missed detection; (c) NMSE and state evolution.

in the SNR=20dB and 30dB cases. These false signals likely contributed to the atypical trend.

6) *Performance on Estimator:* In order to analyze the performance of our AMP algorithm in user detection and channel estimation compared with the state evolution result, we estimate \mathbf{X} from the received signal matrix \mathbf{Y} in (9). In this setting, we fix X with antennas $M = 32$ and change the noise power.

Fig. 6 shows the estimation results of each antenna value using weak noise power (SNR = 50dB) and strong noise power (SNR = 0dB) for GST-AMP, GST-AMP-SE algorithm, HT-AMP, HT-AMP-SE algorithm, and S-AMP, S-AMP-SE algorithm, respectively. This result demonstrates that both numerical simulations can estimate the true value with high precision when the noise power is low, and vice versa.

To evaluate the performance of our estimator under normal settings, we generate an estimate \hat{X} from X by the GST-AMP, HT-AMP and S-AMP algorithm, respectively. We add different noises randomly 10000 times with SNR = 30dB in X and summary the statistics of the NMSE between X and \hat{X} in Fig. 7. It's seen that most of the generated estimates follow the three-sigma rule of thumb law [45], where the results fit the norm distribution with $\mu = 0.046$ and $\sigma = 0.0055$ in GST-AMP, the norm distribution with $\mu = 0.022$ and $\sigma = 0.0028$

in HT-AMP, and the half-norm distribution with $\mu = 0$ and $\sigma = 0.0039$ in S-AMP.

7) *Running Time:* We have measured the average running time for GST-AMP, HT-AMP, S-AMP, and MMSE-AMP algorithms. We have considered the different numbers of channels (M) when $K = 100$, and for varying levels of user activity (K) when $M = 32$.

These results demonstrate the performance of the proposed algorithms in practical scenarios and provide insights into their suitability for varying channel and user activity conditions.

VI. CONCLUSIONS

In this paper, we solved the problem of jointly user activity detection and channel estimation for establishing successful communication between the cellular base stations and the devices. We first proposed a group soft-thresholding AMP detector to exploit only the sparsity in user activity. Then, we proposed a hard-thresholding AMP detector based on the on-grid CS approach by using the user and channel sparsities. Moreover, we proposed a direct SDP solver and a super-resolution AMP detector to solve the off-grid problem, where a greedy method based the atomic norm technique is used as the super-resolution denoiser. We presented the state evolution results of the proposed methods. A large number of experimental results validate the proposed method, which is expected

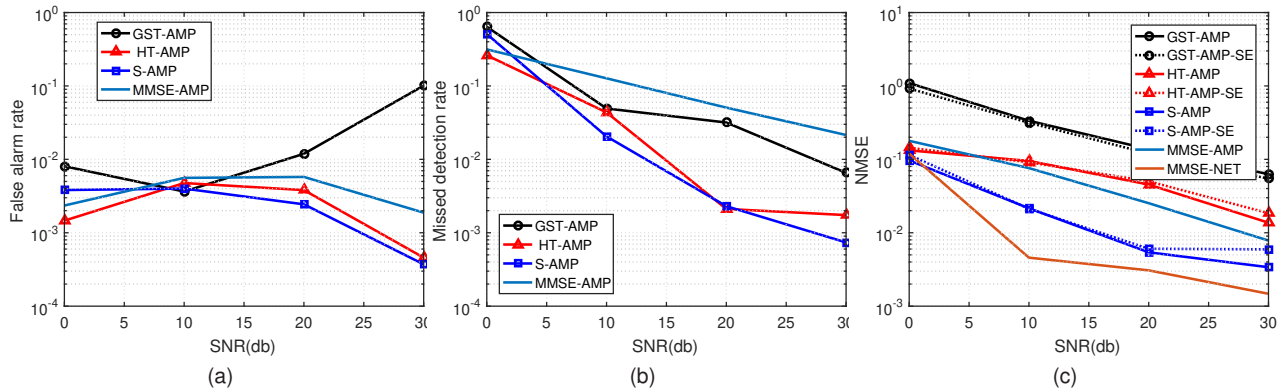


Fig. 5: Numerical simulation results as functions of the length of SNR. (a) False alarm; (b) Missed detection; (c) NMSE and state evolution.

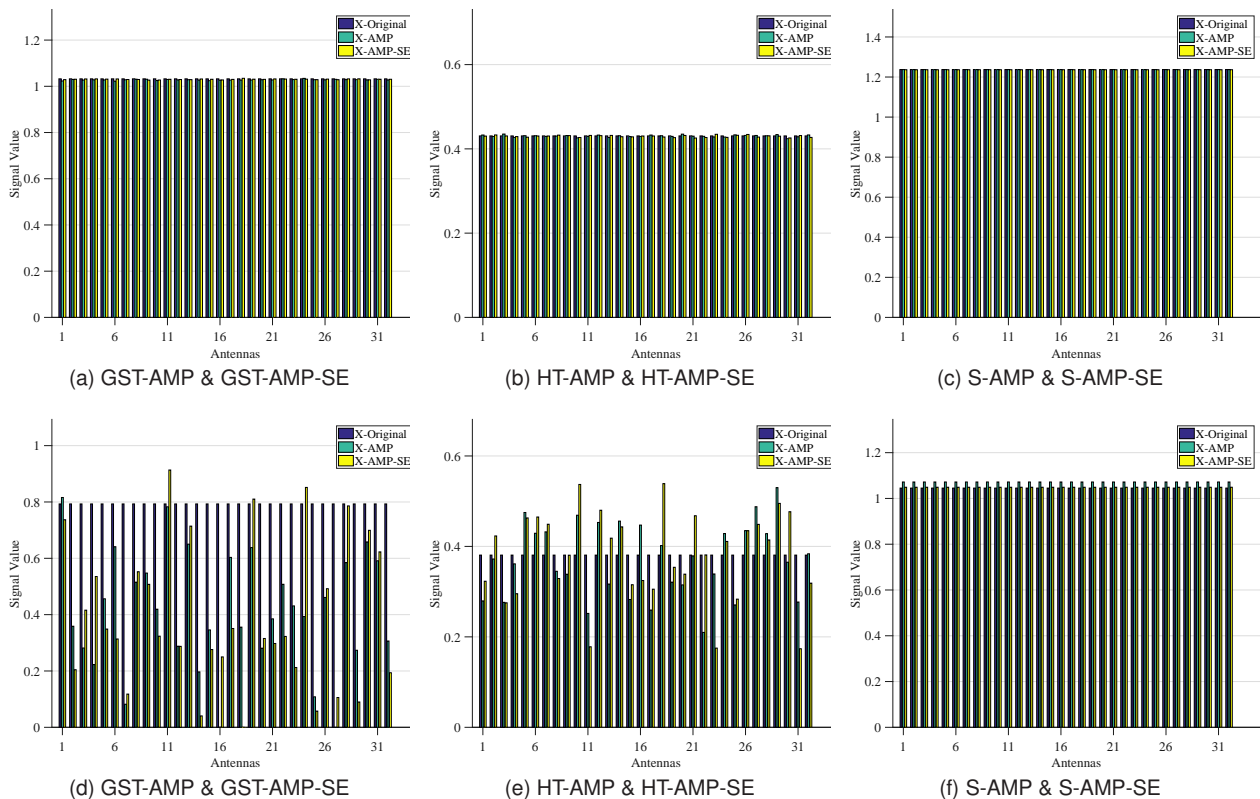


Fig. 6: Estimation of X value with proposed methods. (a)-(c) SNR=50dB. (d)-(e) SNR=0dB.

TABLE II: Running times of the proposed algorithms for the different channel (M) and user activity (K).

Method	channels ($K=100$)				channels ($M=32$)				
	$M=8$	$M=16$	$M=32$	$M=64$	$K=50$	$K=100$	$K=200$	$K=400$	$K=1000$
GST-AMP	0.29 s	0.48 s	0.73 s	1.88 s	0.74 s	0.73 s	0.81 s	0.842 s	0.86 s
HT-AMP	0.24 s	0.29 s	0.47 s	1.36 s	0.48 s	0.47 s	0.49 s	0.54 s	0.55 s
S-AMP	0.74 s	0.70s	0.96 s	2.14 s	0.84 s	0.96 s	2.48 s	4.46 s	10.39 s
MMSE-AMP	0.086 s	0.096 s	0.17 s	0.41 s	0.13 s	0.17 s	0.25 s	0.44 s	0.55 s

to achieve promising performance for user activity detection and channel estimation in B5G or 6G wireless communication networks.

APPENDIX

A. Table of Symbols

We have arranged and listed the symbols that appear in Table III.

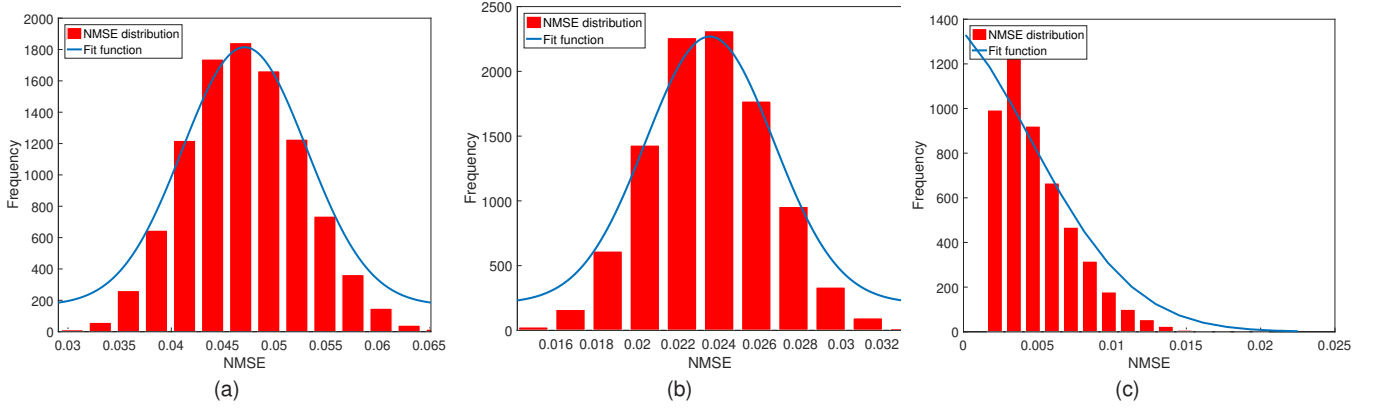


Fig. 7: Statistics NMSE distribution between the X and \hat{X} with SNR=30dB in (a) GST-AMP, (b) HT-AMP and (c) S-AMP, respectively.

TABLE III: Table of Symbols

Symbol	Description
N	Number of users
M	Number of BS antennas
K	Number of active devices
L_n	Number of paths of the n -th user
$\bar{c}_{n,\ell}$	Complex gain of the ℓ -th path of the n -th user
$\mathbf{a}(f)$	Steering vector of the receive array
f	Angle of arrival
d	Separation of adjacent antenna elements
λ_w	Wavelength of the transmitted signal
ϵ	User activity probability
α_n	User activity indicator
\mathbf{u}_n	Data symbols of the n -th user
Q	Length of pilot sequence
ρ	Pilot transmit power
\mathbf{h}_n	Complex uplink channel vector of the n -th user
\mathbf{X}	Matrix of channel vectors
\mathbf{Y}	Matrix of received signal
\mathbf{Z}	Noise matrix
\mathbf{R}^t	Residual matrix at iteration t
\mathbf{x}_n^t	Channel vector of the n -th user at iteration t
$\eta_t(\cdot)$	Non-linear function known as denoiser
β_n	Path-loss and shadowing component of the n -th user
$\tilde{\mathbf{x}}_n^t$	Input argument of the denoiser at iteration t for user n
γ	Weighting parameter
\mathbf{w}_n	Weight vector of the n -th user
$\hat{\mathbf{x}}_n$	Estimate of the n -th user's channel vector
$\hat{\mathbf{X}}$	Estimate of the matrix of channel vectors
$\hat{\mathbf{Y}}$	Estimate of the matrix of received signal
$\hat{\mathbf{Z}}$	Estimate of the noise matrix
$\hat{\mathbf{R}}^t$	Estimate of the residual matrix at iteration t
$\hat{\mathbf{u}}_n$	Estimate of the data symbols of the n -th user

B. Theorem 1

Theorem 1. Denote $\mathbf{d}_{m,1}, \mathbf{d}_{m,2}, \dots, \mathbf{d}_{m,N} \in \mathbb{C}^{M \times 1}$ whose m -th element obeys i.i.d. complex Gaussian distribution $\mathcal{CN}(0, 1)$ and the rest of the elements are zero. Then we have

$$\mathbf{v}_m = \lim_{\epsilon \rightarrow 0} \mathbb{E} \left\{ \frac{1}{\epsilon} \sum_{n=1}^N d_{m,n}(m) (\eta_t(\tilde{\mathbf{x}}_n + \epsilon \mathbf{d}_{m,n}) - \eta_t(\tilde{\mathbf{x}}_n)) \right\}$$

provided that $\eta_t(\cdot)$ admits a well-defined second-order Taylor expansion.

Proof: We write the second-order Taylor expansion of $\eta_t(\tilde{\mathbf{x}} + \epsilon \mathbf{d}_{m,n})$ as

$$\begin{aligned} \eta_t(\tilde{\mathbf{x}}_n + \epsilon \mathbf{d}_{m,n}) &= \eta_t(\tilde{\mathbf{x}}_n) \\ &+ \epsilon \frac{\partial \eta_t(\tilde{\mathbf{x}}_n)}{\partial \tilde{\mathbf{x}}_n(m)} d_{m,n}(m) + \epsilon^2 \mathbf{r}_\eta(\tilde{\mathbf{x}}_n, d_{m,n}(m)). \end{aligned} \quad (42)$$

where $\mathbf{r}_\eta \in \mathbb{C}^{M \times 1}$ is the Lagrange remainder vector, whose each element corresponding to each component of $\eta_t(\cdot)$ and we hence have $\mathbb{E} |\mathbf{r}_\eta(m)| < +\infty$ for $m = 1, 2, \dots, M$.

Then, subtracting $\eta_t(\tilde{\mathbf{x}}_n)$ from (42) and we obtain

$$\begin{aligned} &\mathbb{E} \left\{ \sum_{n=1}^N d_{m,n}(n) [\eta_t(\tilde{\mathbf{x}}_n + \epsilon \mathbf{d}_{m,n}) - \eta_t(\tilde{\mathbf{x}}_n)] \right\} \\ &= \epsilon \mathbb{E} \left\{ \sum_{n=1}^N d_{m,n}^2(n) \frac{\partial \eta_t(\tilde{\mathbf{x}}_n)}{\partial \tilde{\mathbf{x}}_n(m)} \right\} \\ &\quad + \epsilon^2 \mathbb{E} \left\{ \sum_{n=1}^N d_{m,n}(n) \mathbf{r}_\eta(\tilde{\mathbf{x}}_n, d_{m,n}(m)) \right\} \\ &= \epsilon \sum_{n=1}^N \frac{\partial \eta_t(\tilde{\mathbf{x}}_n)}{\partial \tilde{\mathbf{x}}_n(m)} + C_2 \epsilon^2, \end{aligned} \quad (43)$$

where $\mathbb{E} \left\{ \sum_{n=1}^N d_{m,n}(n) \mathbf{r}_\eta(\tilde{\mathbf{x}}_n, d_{m,n}(m)) \right\} = C_2$ and $|C_2| < +\infty$ because $\mathbb{E} \left\{ \mathbf{r}_\eta(\tilde{\mathbf{x}}_n, d_{m,n}(m)) \right\} < +\infty$ for $k = 1, 2, \dots, N$ and $d_{m,n}(n)$ has bounded higher-order moments since $d_{m,n}(n) \sim \mathcal{CN}(0, 1)$. When $\epsilon \rightarrow 0$, we immediately see that

$$\begin{aligned} &\lim_{\epsilon \rightarrow 0} \frac{1}{\epsilon} \mathbb{E} \left\{ \sum_{n=1}^N d_{m,n}(n) [\eta_t(\tilde{\mathbf{x}}_n + \epsilon \mathbf{d}_{m,n}) - \eta_t(\tilde{\mathbf{x}}_n)] \right\} \\ &= \sum_{n=1}^N \frac{\partial \eta_t(\tilde{\mathbf{x}}_n)}{\partial \tilde{\mathbf{x}}_n(m)} = \mathbf{v}_m. \end{aligned} \quad (44)$$

Then we complete the proof. \blacksquare

C. Super-resolution AMP (S-AMP)

- 1) **Initialization:** Define \mathcal{T} as the set of estimated spectral lines, and denote $\mathbf{r}_{\text{res}} \in \mathbb{C}^{M \times 1}$ as a residual. Then, initialize $\mathcal{T} \leftarrow \emptyset$ and $\mathbf{r}_{\text{res}} \leftarrow \tilde{\mathbf{x}}$.
- 2) **Selection:** Compute the atom in \mathcal{A} that has the highest correlation with the current residual \mathbf{r}_{res} and update \mathcal{T} i.e, compute

$$f^\circ = \arg \max_{f \in [0,1]} \text{corr}(f), \quad (45)$$

where $\text{corr}(f) := |\langle \mathbf{a}(f), \mathbf{r}_{\text{res}} \rangle|$ and let $\mathcal{T} \leftarrow \mathcal{T} \cup \{f^\circ\}$. For atoms, we calculate the highest correlation by approximately finding the position of the maximum of $\text{corr}(f)$ on the fine grid f_{grid} . To be more efficient, we can construct the oversampled fast Fourier transform on \mathbf{r}_{res} and directly find the largest element of $\text{corr}(f)$ for $f \in f_{\text{grid}}$.

- 3) **Local optimization:** After \mathcal{T} is updated, define $\mathbf{c} = [c_1, c_2, \dots, c_{|\mathcal{T}|}]^T \in \mathbb{C}^{|\mathcal{T}|}$ and $\mathbf{f} = [f_1, f_2, \dots, f_{|\mathcal{T}|}]^T \in [0, 1]^{|\mathcal{T}|}$ in $\mathbf{x} = \Phi(\mathbf{f})\mathbf{c}$, where

$$\Phi(\mathbf{f}) = [\mathbf{a}(f_1), \mathbf{a}(f_2), \dots, \mathbf{a}(f_{|\mathcal{T}|})] \in \mathbb{C}^{M \times |\mathcal{T}|}. \quad (46)$$

Then, we refine \mathbf{f} in \mathcal{T} by solving

$$\min_{\mathbf{f} \in [0,1]^{|\mathcal{T}|}, \mathbf{c} \in \mathbb{C}^{|\mathcal{T}|}} \|\tilde{\mathbf{x}} - \Phi(\mathbf{f})\mathbf{c}\|_2^2. \quad (47)$$

Substituting the solution $\hat{\mathbf{c}} = \Phi(\mathbf{f})^\dagger \tilde{\mathbf{x}}$ back to (47) yields [46], [47]:

$$\hat{\mathbf{f}} = \arg \min_{\mathbf{f} \in [0,1]^{|\mathcal{T}|}} \text{Tr}\{\mathbf{P}^\perp(\mathbf{f})\mathbf{R}\}, \quad (48)$$

where

$$\mathbf{R} = \tilde{\mathbf{x}}\tilde{\mathbf{x}}^H \in \mathbb{C}^{M \times M}, \quad (49)$$

$$\mathbf{P}^\perp(\mathbf{f}) = \mathbf{I}_M - \Phi(\mathbf{f})\Phi(\mathbf{f})^\dagger \in \mathbb{C}^{M \times M}, \quad (50)$$

and $(\cdot)^\dagger$ denotes the pseudo-inverse, i.e., $\mathbf{X}^\dagger = (\mathbf{X}^H \mathbf{X})^{-1} \mathbf{X}^H$. Next, we calculate the gradient and Hessian matrix as follows [46], [47]

$$\begin{aligned} \mathbf{p}(\mathbf{f}) &= \nabla_{\mathbf{f}} [\text{Tr}\{\mathbf{P}^\perp(\mathbf{f})\mathbf{R}\}] \in \mathbb{R}^{|\mathcal{T}| \times 1} \\ &= -2\Re \{ \text{vec-diag} [\Phi^\dagger(\mathbf{f})\mathbf{R}\mathbf{P}^\perp(\mathbf{f})\mathbf{T}(\mathbf{f})] \}, \end{aligned} \quad (51)$$

$$\begin{aligned} \mathbf{K}(\mathbf{f}) &= \nabla_{\mathbf{f}}^2 [\text{Tr}\{\mathbf{P}^\perp(\mathbf{f})\mathbf{R}\}] \in \mathbb{R}^{|\mathcal{T}| \times |\mathcal{T}|} \\ &\approx 2\Re \{ (\mathbf{T}(\mathbf{f})^H \mathbf{P}^\perp(\mathbf{f})\mathbf{T}(\mathbf{f})) \odot (\Phi(\mathbf{f})^\dagger \mathbf{R} \Phi(\mathbf{f})^\dagger)^H \}, \end{aligned} \quad (52)$$

where $\text{vec-diag}[\cdot]$ denotes the operator that outputs a vector generated by the diagonal elements of an input square matrix, and $\mathbf{T}(\mathbf{f})$ is given by (53)

$$\begin{aligned} \mathbf{T}(\mathbf{f}) &= \left[\frac{\partial \mathbf{a}(f)}{\partial f} \Big|_{f=f_1}, \frac{\partial \mathbf{a}(f)}{\partial f} \Big|_{f=f_2}, \dots, \frac{\partial \mathbf{a}(f)}{\partial f} \Big|_{f=f_{|\mathcal{T}|}} \right] \in \mathbb{C}^{M \times |\mathcal{T}|} \\ &= \begin{bmatrix} 1 & 1 & \dots & 1 \\ i2\pi e^{i2\pi f_1} & i2\pi e^{i2\pi f_2} & \dots & i2\pi e^{i2\pi f_{|\mathcal{T}|}} \\ \vdots & \vdots & \ddots & \vdots \\ i2\pi(M-1)e^{i2\pi(M-1)f_1} & i2\pi(M-1)e^{i2\pi(M-1)f_2} & \dots & i2\pi(M-1)e^{i2\pi(M-1)f_{|\mathcal{T}|}} \end{bmatrix}. \end{aligned} \quad (53)$$

Finally, we solve (48) based on the gradient and Hessian following the Newton's method as

$$\mathbf{f}^{i+1} = \mathbf{f}^i - \mu_i \mathbf{K}(\mathbf{f}^i)^{-1} \mathbf{p}(\mathbf{f}^i), \quad i = 0, 1, \dots \quad (54)$$

where μ_i is a step size, and the iteration goes until the maximum iteration number I is reached or the condition $\|\mathbf{K}(\mathbf{f}^i)^{-1} \mathbf{p}(\mathbf{f}^i)\|_2 < \delta$ is satisfied. The elements in \mathcal{T} are used as the initialization point \mathbf{f}^0 .

- 4) **Least-squares:** Once \mathcal{T} is obtained, we can estimate \mathbf{c} by solving the following least-squares problem:

$$\hat{\mathbf{c}} = \arg \min_{\mathbf{c} \in \mathbb{C}^{|\mathcal{T}|}} \|\tilde{\mathbf{x}} - \Phi(\hat{\mathbf{f}})\mathbf{c}\|_2^2. \quad (55)$$

Based on the estimated coefficients $\hat{\mathbf{c}}$, we remove any atoms in \mathcal{T} whose corresponding coefficients are smaller than a predefined threshold δ .

- 5) **Residual update:**

$$\mathbf{r}_{\text{res}} = \tilde{\mathbf{x}} - \Phi(\hat{\mathbf{f}})\hat{\mathbf{c}} \quad (56)$$

and repeat steps 2) to 5) until $\|\mathbf{r}_{\text{res}}\|_2^2 \leq \epsilon$, or the maximum iteration number I' is reached.

VII. ACKNOWLEDGEMENT

This work was supported by the National Key R&D Program of China (Grant No. 2018YFE0202101, 2018YFE0202103). Le Zheng is the corresponding author.

REFERENCES

- [1] L. Liu and W. Yu, "Massive connectivity with massive MIMO-Part I: Device activity detection and channel estimation," *IEEE Transactions on Signal Processing*, vol. 66, no. 11, pp. 2933–2946, 2018.
- [2] —, "Massive connectivity with massive MIMO-Part II: Achievable rate characterization," *IEEE Transactions on Signal Processing*, vol. 66, no. 11, pp. 2947–2959, 2018.
- [3] —, "Massive device connectivity with massive MIMO," in *2017 IEEE International Symposium on Information Theory (ISIT)*. IEEE, 2017, pp. 1072–1076.
- [4] M. Hasan, E. Hossain, and D. Niyato, "Random access for machine-to-machine communication in LTE-advanced networks: Issues and approaches," *IEEE communications Magazine*, vol. 51, no. 6, pp. 86–93, 2013.
- [5] E. Björnson, E. De Carvalho, J. H. Sørensen, E. G. Larsson, and P. Popovski, "A random access protocol for pilot allocation in crowded massive MIMO systems," *IEEE Transactions on Wireless Communications*, vol. 16, no. 4, pp. 2220–2234, 2017.
- [6] H. Zhu and G. B. Giannakis, "Exploiting sparse user activity in multiuser detection," *IEEE Transactions on Communications*, vol. 59, no. 2, pp. 454–465, 2010.
- [7] H. F. Schepker and A. Dekorsy, "Compressive sensing multi-user detection with block-wise orthogonal least squares," in *2012 IEEE 75th Vehicular Technology Conference (VTC Spring)*. IEEE, 2012, pp. 1–5.

- [8] X. Xu, X. Rao, and V. K. Lau, "Active user detection and channel estimation in uplink CRAN systems," in *2015 IEEE International Conference on Communications (ICC)*. IEEE, 2015, pp. 2727–2732.
- [9] G. Wunder, P. Jung, and M. Ramadan, "Compressive random access using a common overloaded control channel," in *2015 IEEE Globecom Workshops (GC Wkshps)*. IEEE, 2015, pp. 1–6.
- [10] H. F. Schepker, C. Bockelmann, and A. Dekorsy, "Exploiting sparsity in channel and data estimation for sporadic multi-user communication," in *ISWCS 2013; The Tenth International Symposium on Wireless Communication Systems*. VDE, 2013, pp. 1–5.
- [11] G. Wunder, H. Boche, T. Strohmer, and P. Jung, "Sparse signal processing concepts for efficient 5G system design," *IEEE Access*, vol. 3, pp. 195–208, 2015.
- [12] G. Hannak, M. Mayer, A. Jung, G. Matz, and N. Goertz, "Joint channel estimation and activity detection for multiuser communication systems," in *2015 IEEE International Conference on Communication Workshop (ICCW)*. IEEE, 2015, pp. 2086–2091.
- [13] Z. Chen, F. Sahrabi, and W. Yu, "Sparse activity detection for massive connectivity," *IEEE Transactions on Signal Processing*, vol. 66, no. 7, pp. 1890–1904, 2018.
- [14] W. Chen, H. Xiao, L. Sun, and B. Ai, "Joint activity detection and channel estimation in massive mimo systems with angular domain enhancement," *IEEE Transactions on Wireless Communications*, vol. 21, no. 5, pp. 2999–3011, 2021.
- [15] M. Bayati and A. Montanari, "The dynamics of message passing on dense graphs, with applications to compressed sensing," *IEEE Transactions on Information Theory*, vol. 57, no. 2, pp. 764–785, 2011.
- [16] Z. Chen and W. Yu, "Massive device activity detection by approximate message passing," in *2017 IEEE International Conference on Acoustics, Speech and Signal Processing (ICASSP)*. IEEE, 2017, pp. 3514–3518.
- [17] J. Johnston and X. Wang, "Model-based deep learning for joint activity detection and channel estimation in massive and sporadic connectivity," *IEEE Transactions on Wireless Communications*, vol. 21, no. 11, pp. 9806–9817, 2022.
- [18] X. Ma, Z. Gao, F. Gao, and M. Di Renzo, "Model-driven deep learning based channel estimation and feedback for millimeter-wave massive hybrid mimo systems," *IEEE Journal on Selected Areas in Communications*, vol. 39, no. 8, pp. 2388–2406, 2021.
- [19] G. Tang, B. N. Bhaskar, P. Shah, and B. Recht, "Compressed sensing off the grid," *IEEE transactions on information theory*, vol. 59, no. 11, pp. 7465–7490, 2013.
- [20] D. L. Donoho, "Compressed sensing," *IEEE Trans. Inf. Theory*, vol. 52, no. 4, pp. 1289–1306, 2006.
- [21] E. J. Candes, Y. C. Eldar, D. Needell, and P. Randall, "Compressed sensing with coherent and redundant dictionaries," *Appl. Comput. Harmon. Anal.*, vol. 31, no. 1, pp. 59–73, 2011.
- [22] L. Stanković, I. Orović, S. Stanković, and M. Amin, "Compressive sensing based separation of nonstationary and stationary signals overlapping in time-frequency," *IEEE Transactions on Signal Processing*, vol. 61, no. 18, pp. 4562–4572, 2013.
- [23] C. Studer, P. Kuppinger, G. Pope, and H. Bolcskei, "Recovery of sparsely corrupted signals," *IEEE Transactions on Information Theory*, vol. 58, no. 5, pp. 3115–3130, 2012.
- [24] Y. Li, X. Wang, and Z. Ding, "Multi-target position and velocity estimation using ofdm communication signals," *IEEE Transactions on Communications*, vol. 68, no. 2, pp. 1160–1174, 2019.
- [25] Y. Li, L. Zheng, M. Lops, and X. Wang, "Interference removal for radar/communication co-existence: The random scattering case," *IEEE Transactions on Wireless Communications*, vol. 18, no. 10, pp. 4831–4845, 2019.
- [26] Z. Yang and L. Xie, "Exact joint sparse frequency recovery via optimization methods," *IEEE Trans. Signal Process.*, vol. 64, no. 19, pp. 5145–5157, 2014.
- [27] B. N. Bhaskar, G. Tang, and B. Recht, "Atomic norm denoising with applications to line spectral estimation," *IEEE Trans. Signal Process.*, vol. 61, no. 23, pp. 5987–5999, Dec. 2013.
- [28] Y. Li, X. Wang, and Z. Ding, "Multi-dimensional spectral super-resolution with prior knowledge with application to high mobility channel estimation," *IEEE Journal on Selected Areas in Communications*, 2020.
- [29] C. A. Metzler, A. Maleki, and R. G. Baraniuk, "From denoising to compressed sensing," *IEEE Transactions on Information Theory*, vol. 62, no. 9, pp. 5117–5144, 2016.
- [30] S. Ramani, T. Blu, and M. Unser, "Monte-Carlo SURE: A black-box optimization of regularization parameters for general denoising algorithms," *IEEE Transactions on Image Processing*, vol. 17, no. 9, pp. 1540–1554, 2008.
- [31] A. Alkhateeb, O. El Ayach, G. Leus, and R. W. Heath, "Channel estimation and hybrid precoding for millimeter wave cellular systems," *IEEE Journal of Selected Topics in Signal Processing*, vol. 8, no. 5, pp. 831–846, 2014.
- [32] Z. Xiao, P. Xia, and X.-G. Xia, "Channel estimation and hybrid precoding for millimeter-wave mimo systems: A low-complexity overall solution," *IEEE Access*, vol. 5, pp. 16 100–16 110, 2017.
- [33] J. Kim, W. Chang, B. Jung, D. Baron, and J. C. Ye, "Belief propagation for joint sparse recovery," *arXiv preprint arXiv:1102.3289*, 2011.
- [34] L. Zheng, A. Maleki, H. Weng, X. Wang, and T. Long, "Does ℓ_p -minimization outperform ℓ_1 -minimization?" *IEEE Transactions on Information Theory*, vol. 63, no. 11, pp. 6896–6935, 2017.
- [35] A. Javanmard and A. Montanari, "State evolution for general approximate message passing algorithms, with applications to spatial coupling," *Information and Inference: A Journal of the IMA*, vol. 2, no. 2, pp. 115–144, 2013.
- [36] T. L. Marzetta, "Noncooperative cellular wireless with unlimited numbers of base station antennas," *IEEE Transactions on Wireless Communications*, vol. 9, no. 11, pp. 3590–3600, 2010.
- [37] C. Guo and M. E. Davies, "Near optimal compressed sensing without priors: Parametric sure approximate message passing," *IEEE Trans. Signal Processing*, vol. 63, no. 8, pp. 2130–2141, 2015.
- [38] L. Zheng, Z. Wu, M. Seok, X. Wang, and Q. Liu, "High-accuracy compressed sensing decoder based on adaptive (ℓ_0, ℓ_1) complex approximate message passing: Cross-layer design," *IEEE Transactions on Circuits and Systems I: Regular Papers*, vol. 63, no. 10, pp. 1726–1736, 2016.
- [39] S. Boyd and L. Vandenberghe, *Convex optimization*. Cambridge, U.K.: Cambridge Univ. Press, 2004.
- [40] J. F. Sturm, "Using SeDuMi 1.02, a MATLAB toolbox for optimization over symmetric cones," *Optimization Methods and Software*, vol. 11, no. 1-4, pp. 625–653, 1999.
- [41] K.-C. Toh, M. J. Todd, and R. H. Tütüncü, "SDPT3—a MATLAB software package for semidefinite programming, version 1.3," *Optimization Methods and Software*, vol. 11, no. 1-4, pp. 545–581, 1999.
- [42] A. Eftekhari and M. B. Wakin, "Greed is super: A fast algorithm for super-resolution," *arXiv preprint arXiv:1511.03385*, 2015.
- [43] A. Fannjiang and W. Liao, "Coherence pattern-guided compressive sensing with unresolved grids," *SIAM Journal on Imaging Sciences*, vol. 5, no. 1, pp. 179–202, 2012.
- [44] L. Zheng, M. Lops, and X. Wang, "Adaptive interference removal for uncoordinated radar/communication coexistence," *IEEE J. Sel. Top. Signal Process.*, vol. 12, no. 1, pp. 45–60, 2018.
- [45] F. Pukelsheim, "The three sigma rule," *The American Statistician*, vol. 48, no. 2, pp. 88–91, 1994.
- [46] M. Viberg, B. Ottersten, and T. Kailath, "Detection and estimation in sensor arrays using weighted subspace fitting," *IEEE Trans. Signal Process.*, vol. 39, no. 11, pp. 2436–2449, 1991.
- [47] M. Viberg and B. Ottersten, "Sensor array processing based on subspace fitting," *IEEE Trans. Signal Process.*, vol. 39, no. 5, pp. 1110–1121, 1991.